



ORIGINAL RESEARCH ARTICLE

# Effects of Pressure Holding Time on Magnetic Properties and Corrosion Resistance of Hot-Deformed NdFeB Magnets

Xiaoqiang Li, Junjie Ni, Zhiwei Wang, Bo Song, Changzheng Wang, and Xigui Cui

Submitted: 31 May 2023 / Revised: 12 July 2023 / Accepted: 22 July 2023 / Published online: 7 August 2023

Effects of pressure holding time (PHT) on magnetic properties and electrochemical corrosion behavior of hot-deformed NdFeB were investigated through x-ray diffraction, x-ray photoelectron spectrometer, scanning electron microscopy, and magnetic and anti-corrosion properties measurement technologies. 10 min PHT has been found to increase the orientation degree of matrix phase with only slight grain growth. When PHT is increased up to 40 min, however, the platelet-shaped grains obviously grow along their length direction, reducing the magnet orientation degree and worsening the distribution of Nd-rich phases. Compared to the magnet without and with longer PHT, the magnet with 10 min PHT possesses more appropriate microstructure and better magnetic/anti-corrosion properties. The increase in the intrinsic coercivity and magnetic energy product is 17.4 and 14.2%, respectively. The improved corrosion resistance is due to the difficult formation of active reaction channels in Nd-rich phases induced by their optimized distribution. Such novel findings can provide some theoretical and experimental information for improving the performance of hot-deformed NdFeB.

**Keywords** corrosion resistance, magnetic properties, microstructure, NdFeB

## 1. Introduction

Hot-deformed (HD) NdFeB magnets with a lower content of rare earths than sintered ones have commercially been available for many years. Such magnets are composed of well-aligned platelet-shaped  $\text{Nd}_2\text{Fe}_{14}\text{B}$  ultrafine grains, misaligned coarse grains, strip-shaped Nd-rich phases and grain boundary Nd-rich phases (Ref 1). Their fabrication processes contain melt-spun, hot pressing and hot deformation, in which the deformation speed, degree, temperature and pressure are key preparation parameters to affect the microstructure and grain alignment of highly textured HD magnets (Ref 2). In general, the elevated deformation temperature increases the thickness and length of platelet-shaped ultrafine grains, whose sizes can even be increased from dozens of nanometers to several microns at  $850 \sim 950 \text{ }^\circ\text{C}$  (Ref 3). The grain excessive growth severely retards the deformation of matrix phase and reduces the numbers of grain boundaries, worsening the distribution of Nd-rich phases. Such phases are extruded from HD magnets during deformation process if the temperature exceeds  $850 \text{ }^\circ\text{C}$ , thus decreasing the magnetic properties excessively. Anyway, the deformation temperature

should be controlled to avoid the abnormal grain growth and it often is chosen from  $750$  to  $850 \text{ }^\circ\text{C}$ .

In addition to the temperature, the time factors are another important parameter to affect the magnet microstructure, because hot deformation of NdFeB magnets follows the diffusion creep mechanism (Ref 4) and the diffusion process is related to deformation time and pressure holding time (PHT). The former time factor determines deformation speed, and they have a reverse variation relationship. Their effects on the magnetic properties have been investigated in References (Ref 5, 6), in which Huang et al found a high deformation speed corresponding to short deformation time cannot achieve the sufficient mass transport and good grain orientation. But long deformation time, i.e., low deformation speed, causes the grain excessive growth. This indicates that reasonable selection of deformation time is necessary to obtain high magnetic properties. Similar to the above requirement, PHT needs to be appropriately chosen as well, because the pressure maintenance as a preparation process in powder metallurgy has an impact on the materials microstructure. Unfortunately so far, there are lack of investigations relating PHT effects on the microstructure, magnetic and anti-corrosion properties of hot-deformed NdFeB, which impels us to conduct the related researches for obtaining novel information. In the present works, the material structure–property relationships were discussed on the basis of magnet fabrications with different PHT.

## 2. Experimental

Commercial MQU-F magnetic powders purchased from Magnequench (Tianjin) Co., Ltd. had a composition of  $\text{Nd}_{30.6}\text{Pr}_{0.1}\text{Ga}_{0.45}\text{Co}_{4.0}\text{Fe}_{\text{bal}}\text{B}_{0.9}$  (wt.%), and such raw powders were first compacted in vacuum atmosphere of  $\sim 4.5 \times 10$

Xiaoqiang Li, Junjie Ni, Zhiwei Wang, Bo Song, and Changzheng Wang, School of Materials Science and Engineering, Liaocheng University, Liaocheng 252000, China; and Xigui Cui, School of Mechanical Engineering, Jiangsu University, Zhenjiang 212013, China. Contact e-mail: nijunjie@lcu.edu.cn.

4 Pa under 100 MPa and 680 °C for 30 min to obtain the fully dense precursors. Then, such precursors were hot-deformed at 750 °C with a height reduction by 70% and a deformation speed of  $0.001 \text{ S}^{-1}$ . After deformation, the pressure reached 100 MPa, under which PHT was 0, 10, 20 and 40 min, respectively. Afterward, the as-deformed magnets were annealed at 600 °C for 2 h in a vacuum heat treatment furnace. For the resulting magnets, they are abbreviated as 0PHT, 10PHT, 20PHT and 40PHT magnet when PHT was 0, 10, 20 and 40 min, respectively, in the following sections. Measurement samples of  $10 \times 10 \times 8 \text{ mm}^3$  were taken from their center using a wire-cut machine measurement. Here, surfaces of  $10 \times 8$  and  $10 \times 10 \text{ mm}^2$  were the surfaces parallel and perpendicular to the applied pressure direction, respectively, which were often named as the parallel surface and perpendicular surface. Such surfaces were mechanically ground with SiC paper, polished with diamond paste ( $0.5 \mu\text{m}$ ) and then ultrasonically cleaned by alcohol.

Magnetic properties and electrochemical corrosion performance were, respectively, measured by NIM-10000H magnetic measurement device and CHI660E electrochemical workstation with three electrode cell consisting of Pt counter electrode, saturated calomel reference electrode and NdFeB working electrode. Corrosion evaluations including potentiodynamic polarization curve and electrochemical impedance spectroscopy (EIS) were conducted in 3.5 wt.% NaCl aqueous solution at  $25 \pm 0.2 \text{ }^\circ\text{C}$ . Before polarization measurement, open-circuit potential was monitored for 30 min to make the working electrode in a stable state. Polarization scan was commenced from the negative potential to positive one with a scanning rate of  $2.0 \text{ mV/s}$ . EIS was measured in the frequency range from  $10^5$  to  $10^{-2} \text{ Hz}$  with a signal amplitude perturbation of  $10 \text{ mV}$ . All electrochemical tests were performed seven times in each case. After corrosion, the specimen surface was observed by scanning electron microscope (SEM, ZEISS MERLIN Compact). X-ray photoelectron spectrometer (XPS, ESCALAB250-xi), in which Al  $K\alpha$  was used as the x-ray source (1486.6 eV), was employed to evaluate the corrosion products. In XPS test, x-ray spot size was  $500 \mu\text{m}$ , pressure in the analysis chamber was  $2 \times 10^{-7} \text{ bar}$  and the pass energy was 30 eV. The XPS peaks were fitted using Avantage software.

Fracture morphology in the parallel surface was observed by SEM to investigate the grain growth of  $\text{Nd}_2\text{Fe}_{14}\text{B}$  matrix phase as a function of PHT. The grain sizes were measured by Nano Measurer software. X-ray diffraction (XRD) was used to analyze the texture orientation of magnets with Cu  $K\alpha$  radiation to the perpendicular surface.

## 3. Results and Discussion

### 3.1 Microstructure and Magnetic Properties

Fracture surface of the magnets without and with different PHT is shown in Fig. 1(a), (b), (c) and (d), in which the grains grow slowly in the direction parallel to pressure corresponding to the magnetically easy axis of matrix phase. The grains grow rapidly in the direction perpendicular to pressure, resulting in a platelet-shaped  $\text{Nd}_2\text{Fe}_{14}\text{B}$  grains. Herein, the preferential and non-preferential directions correspond to the directions along length and thickness of  $\text{Nd}_2\text{Fe}_{14}\text{B}$  platelet, respectively. The preferential grain growth is stress-induced via a dissolution–

precipitation mechanism (Ref 7). Also from the fracture surface, ones can observe the size increase in the grain length and thickness with PHT extension. The average sizes of thickness and length are 81 and 285 nm, respectively, for 0PHT magnet, as presented in Fig. 1(e). Both parameters are slightly increased by 10 min PHT, but they have obviously been improved up to 100 and 468 by 20 min PHT, whose growth rate reaches 23.5% and 64.2%, respectively. It indicates that in the latter case, PHT affects the preferential growth direction more significantly compared to the non-preferential growth direction of platelet-shaped  $\text{Nd}_2\text{Fe}_{14}\text{B}$  grains. Over 20 min PHT, the grain growth rate tends to have a small value again and the grains of 40PHT magnet have a thickness of  $\sim 104 \text{ nm}$  and a length of  $\sim 490 \text{ nm}$ . Such phenomena reveal that once PHT exceeds 20 min, the time factor has a little effect on the grain growth behavior. It is said that in 40PHT magnet, there exists abnormal grain growth which coupled with a slight increase in the average grain size is responsible for the reduction in the intrinsic coercivity  $H_{cj}$  from 12.07 kOe for 20PHT magnet to 11.04 kOe for 40PHT magnet (Fig. 2), due in main to the inverse relationship between  $H_{cj}$  and grain size (Ref 8). This reason also accounts for the slight coercivity decrease with the PHT increase from 0 to 10 min. Similarly, the obvious coercivity decrease as a function of PHT from 10 to 20 min is attributed to the remarkable grain growth.

In addition to  $H_{cj}$  in Fig. 2(b), other parameters including remanence  $B_r$ , maximum magnetic energy product  $(BH)_{\text{max}}$ , comprehensive magnetic properties  $(BH)_{\text{max}} + H_{cj}$  and the squareness characterized by the ratio of  $H_k/H_{cj}$  can be obtained from the demagnetization curves in Fig. 2(a), where  $H_k$  is the knee field. It is clear that  $B_r$ ,  $(BH)_{\text{max}}$ ,  $(BH)_{\text{max}} + H_{cj}$  and  $H_k/H_{cj}$  first increase with the PHT extension, respectively, reaching 13.06 kGs, 40.61 MGOe, 53.57 kOe + MGOe and 87.2% at PHT = 10 min, and then decrease by 4.2, 12.4, 13.0 and 6.4% with further PHT extension to 40 min. Among the parameters,  $(BH)_{\text{max}}$  is the main factor to affect  $(BH)_{\text{max}} + H_{cj}$ , considering their similar changing trends and the continuous decline of  $H_{cj}$  as a function of PHT.  $(BH)_{\text{max}}$  depends on  $B_r$  and  $H_k/H_{cj}$  according to  $(BH)_{\text{max}} = \frac{H_k B_r^2}{4H_{cj}}$ , in which the remanence has a greater impact on magnetic energy product compared to the squareness (Ref 9). Aiming to explain the changes in remanence, XRD patterns of magnets were measured and the resulting data are presented in Fig. 3. It is obvious that there are clear (00*i*, *i* = 4, 6, 8) peaks and a small (105) peak, representing the good grain alignment for the test magnets. However, they have different orientation degree, as inferred from the fact that  $I_{(006)}/I_{(105)}$  ratio increases from 1.65 at PHT = 0 min to 1.94 at PHT = 10 min and then decreases to 1.64 at PHT = 40 min. Here,  $I_{(006)}$  and  $I_{(105)}$  are the x-ray diffraction peak intensity, respectively, corresponding to (006) and (105) crystal planes of  $\text{Nd}_2\text{Fe}_{14}\text{B}$  phase.  $I_{(006)}/I_{(105)}$  is often used to characterize the grain orientation degree, and there is a positive correlation between them (Ref 10). This, together with the aforementioned changes of  $I_{(006)}/I_{(105)}$ , means the strongest orientation degree appeared in 10PHT magnet, which accounts for the occurrence of maximum value for  $B_r$  in this magnet because the improved grain orientation has a positive effect on the remanence.

### 3.2 Electrochemical Corrosion Resistance

Figure 4(a) presents Tafel curves of the magnets in 3.5wt.% NaCl aqueous solution. All the curves, from which corrosion

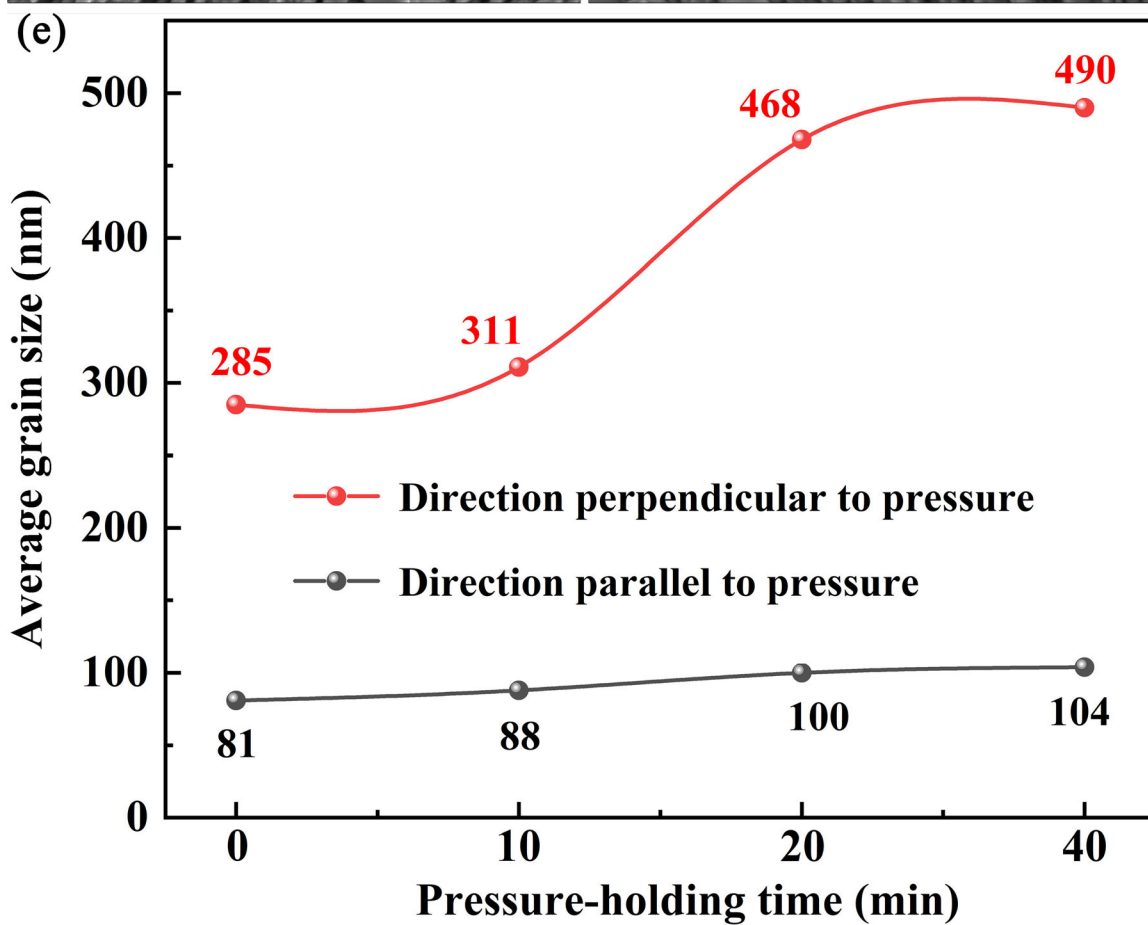
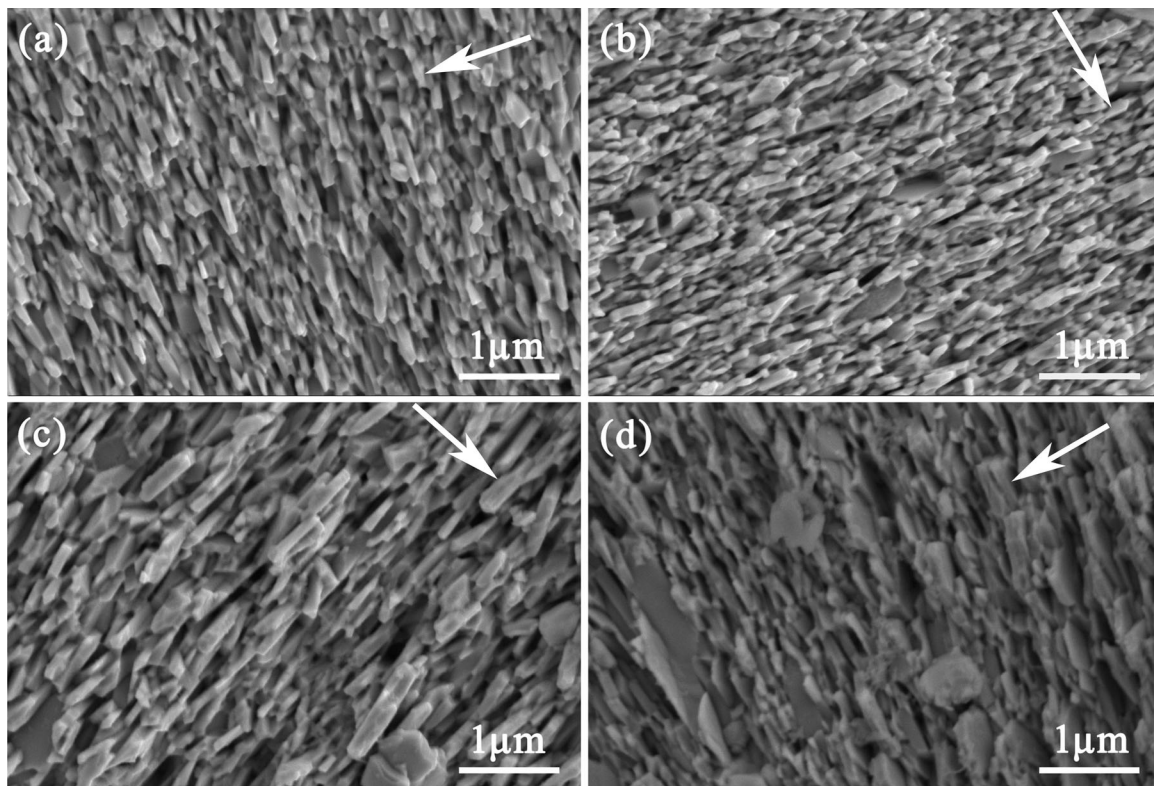


**Fig. 1** SEM micrographs of fracture surfaces of magnets with different pressure holding time: (a) 0 min, (b) 10 min, (c) 20 min, (d) 40 min; (e) change of grain size as a function of pressure holding time. The arrow indicates the pressure direction.

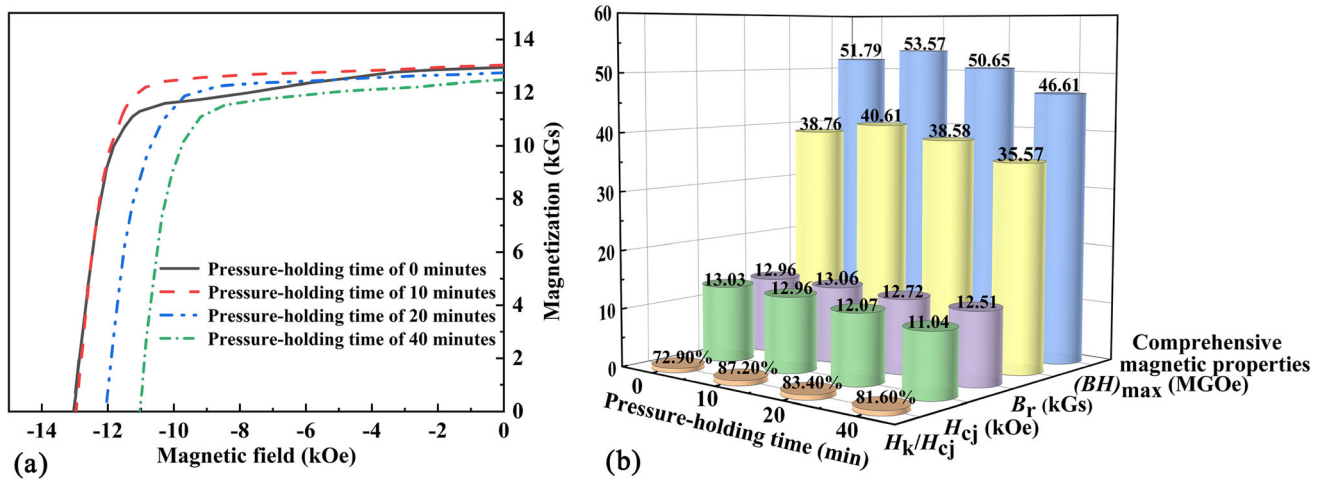


Fig. 2 (a) Demagnetization curves and (b) magnetic parameters and the squareness of magnets

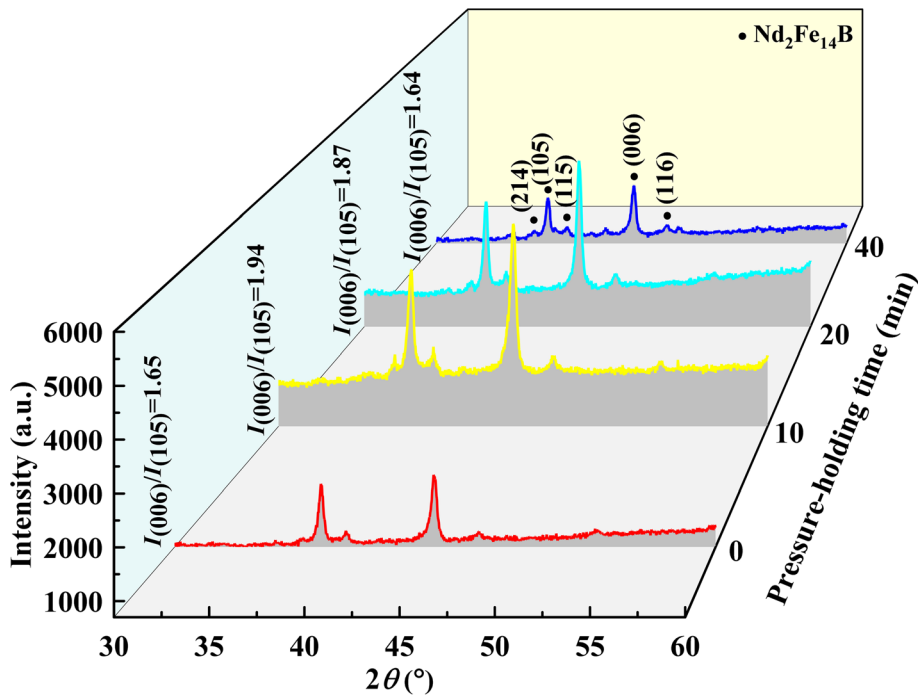
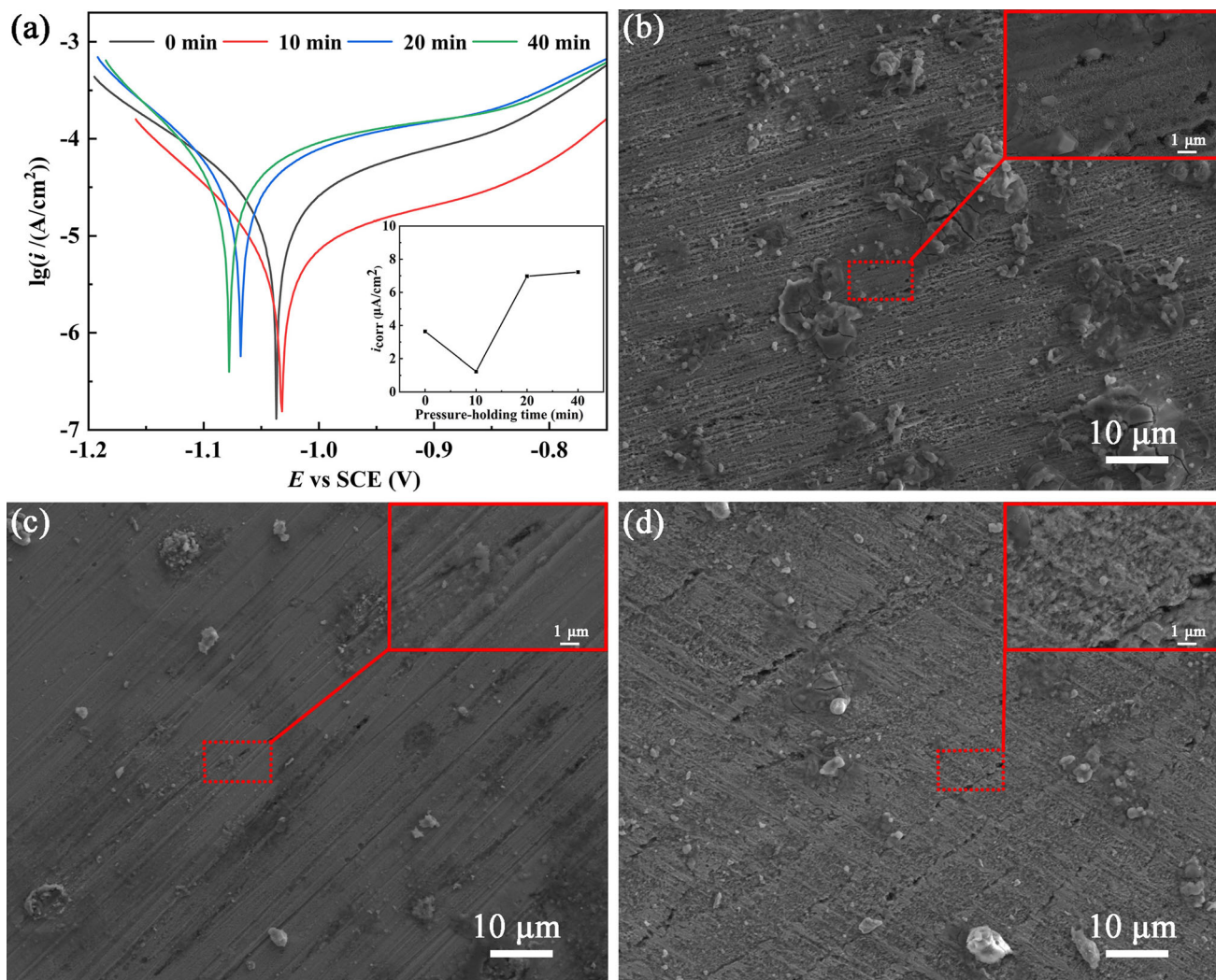


Fig. 3 XRD patterns of magnets with different pressure holding time

current density  $i_{\text{corr}}$  shown in the inset of Fig. 4(a) can be obtained by the Tafel slope extrapolation method, have similar shape, implying that PHT does not change the electrochemical corrosion mechanism of magnets in the test solution. However, the increased PHT reduces  $i_{\text{corr}}$  from 3.64 mA/cm<sup>2</sup> for 0PHT magnet to 1.23 mA/cm<sup>2</sup> for 10PHT magnet and subsequently increases it up to 7.22 mA/cm<sup>2</sup> for 40PHT magnet. It thus is stated that 10PHT magnet possesses a higher corrosion resistance than other samples without pressure holding and with PHT of 20 or 40 min, which is also evidenced by the difference in their corrosion surface (Fig. 4b, c and d). For 0PHT magnet, a large area in magnet surface is dissolved to form a gully-shaped corrosion zone, in which the deep pits are left after the corrosion of strip-shaped Nd-rich phases. For 10PHT magnet, however, most magnet surfaces have not undergone the dissolution except for a few areas where

corrosion occurred, which is attributed to the more uniform distribution of Nd-rich phases as inferred from better grain alignment than the case of 0PHT magnet. Compared to the above two cases, the surface of 40PHT magnet is corroded more seriously, which is related to the agglomeration of Nd-rich phases induced mainly by the remarkable grain growth and the decrease in the number of grain boundaries. The Nd-rich phase agglomeration promotes the formation of active reaction channels in the ribbon boundaries and intergranular regions (Ref 11). It further accelerates the dissolution of Nd-rich phases, leading to the detachment of Nd<sub>2</sub>Fe<sub>14</sub>B matrix phase from magnet substrate. To investigate the corrosion reactions, XPS was measured on the corrosion surfaces of magnets. The results relating to high-resolution spectra of Fe 2p<sub>5/2</sub> and Nd 3d<sub>3/2</sub> are displayed in Fig. 5, from which the peak area ratio of corrosion products corresponding to their content can be



**Fig. 4** (a) Polarization curves of magnets in 3.5 wt.% NaCl aqueous solution, the inset represents the changes of corrosion current density as a function of pressure holding time; corrosion surface morphology of magnets with different pressure holding time: (b) 0 min, (c) 10 min, (d) 40 min

obtained by applying Savitzky–Golay functions to analyze the XPS data. It is obvious that, in addition to the unreacted Fe and Nd, the oxides ( $\text{Nd}_2\text{O}_3$ ,  $\text{Fe}_2\text{O}_3$ ,  $\text{Fe}_3\text{O}_4$ ) and hydroxide of  $\text{Nd}(\text{OH})_3$  distribute in the corrosion layer of all samples. Among them,  $\text{Nd}(\text{OH})_3$  is the reaction products of  $\text{NdH}_3$  and  $\text{H}_2\text{O}$  according to Eqs 1 and 2 (Ref 12). It also can be from the connection of  $\text{Nd}^{3+}$  and  $\text{OH}^-$ . This hydroxide subsequently undergo decomposition reactions forming  $\text{Nd}_2\text{O}_3$ , which is the oxidation products of matrix phase as well (Eq 3).  $\text{Fe}_2\text{O}_3$  and  $\text{Fe}_3\text{O}_4$  are the oxides of Fe. The former distributes in the outer layer of a bilayer structured passive film formed on iron, while  $\text{Fe}_3\text{O}_4$  distributes in the inner layer (Ref 13). Moreover, observations of Fig. 5 allow to see the highest phase percentage of Nd and Fe at PHT = 10 min, indicating a higher resistance of 10PHT magnet against corrosive oxidation than other samples.

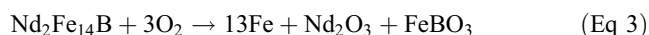
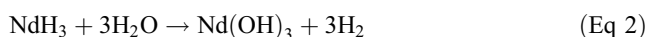
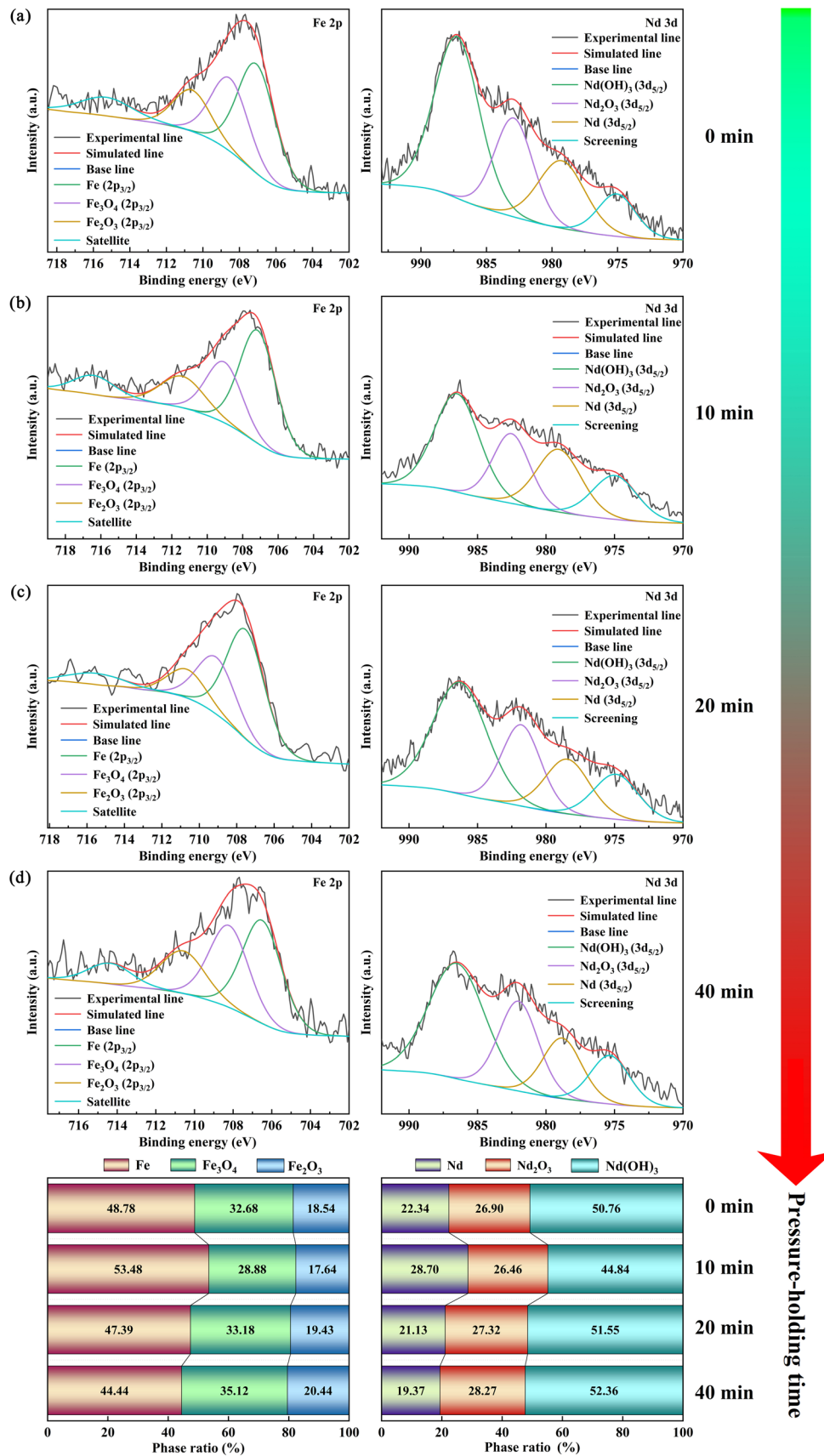
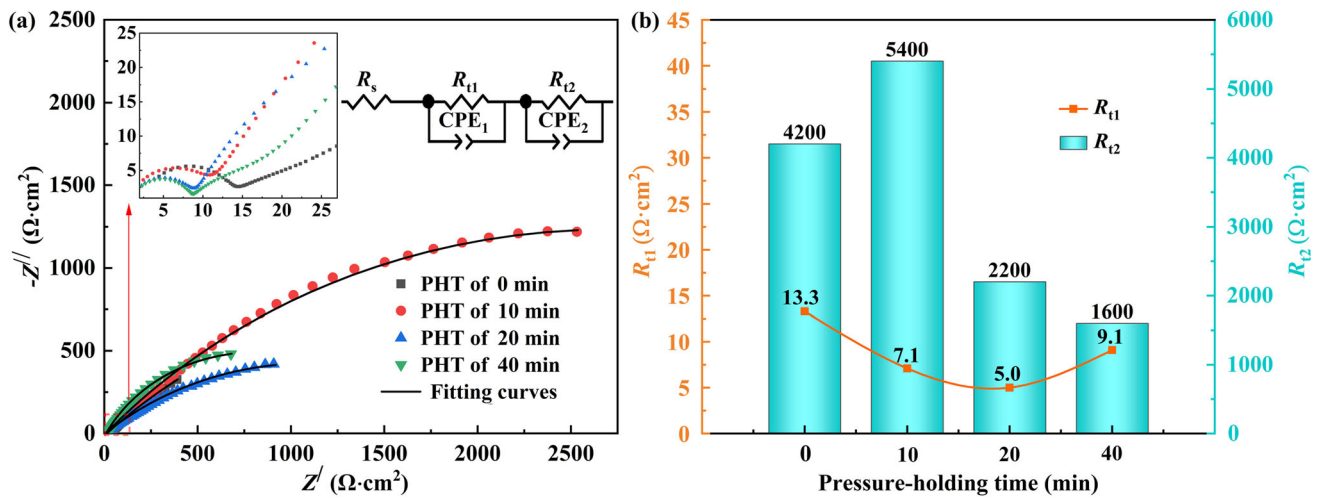


Figure 6(a) shows Nyquist plots of specimens to provide the information relating to the interface corrosion reactions. Such plots include two capacitive loops from high to low frequencies and their equivalent circuit model after data fitting using ZView software is inserted in Fig. 6(a). Herein,  $R_s$ ,  $R_{t1}$  and  $R_{t2}$  refer to the electrolyte resistance, the resistance of corrosion product films and the charge transfer resistance in electric double-layer structure, respectively.  $\text{CPE}_1$  is a constant phase element that is relevant to the characteristics of corrosion product films. It together with  $R_{t1}$  describes the first high-frequency captive loop with a small diameter, indicating that a loose layer on the magnet surface occurs in corrosion.  $R_{t2}$  and  $\text{CPE}_2$  describe the second captive loop, in which  $\text{CPE}_2$  is a constant phase element associate with the magnet surface reactivity, roughness and current distributions. Of the electric elements,  $R_{t1}$  and  $R_{t2}$  are the key parameters and their fitted values are given in Fig. 6(b). Obviously, the value of  $R_{t2}$  is 2 ~ 3 orders of magnitude larger than that of  $R_{t1}$ , which means that the electrochemical corrosion reactions are controlled by charge transfer process in an electric



**Fig. 5** High-resolution x-ray photoelectron spectra of Fe 2p and Nd 3d for the magnets and phase percentage of corrosion products of Nd and Fe for different holding times



**Fig. 6** (a) Nyquist plots and their equivalent circuits of magnets in 3.5 wt.% NaCl aqueous solution; (b) resistance of corrosion product films  $R_1$  and charge transfer resistance  $R_2$  in the equivalent circuit models

double-layer structure. In such processes, the charge transfer capability will be weakened by the amount reduction of active reaction channels in Nd-rich phases, which accounts for the  $R_{t2}$  increase from 1600  $\Omega \cdot \text{cm}^2$  for 40PHT magnet to 5400  $\Omega \cdot \text{cm}^2$  for 10PHT magnet. It, coupled with the reverse relations between the resistance and current, is responsible for a lower  $i_{\text{corr}}$  and stronger corrosion resistance of the latter magnet.

## 4. Conclusions

PHT of 10 min is appropriate for increasing the orientation degree of matrix phase with the slight grain growth, resulting in the enhancement of comprehensive magnetic properties. Extension of PHT up to 20 min and 40 min, however, causes the excessive growth along the length direction of platelet-shaped grains, which reduces the magnet orientation degree and worsens the distribution of Nd-rich phases. It is responsible for obviously lower magnetic properties and electrochemical corrosion resistance of 40PHT magnet compared to 10PHT magnet. The better anti-corrosion property 10PHT magnet is due to the difficult formation of active reaction channels in Nd-rich phases induced by their optimized distribution.

## Acknowledgments

This work was supported by the Natural Science Foundation of Shandong Province of China (Grant No. ZR2021ME031), the National Natural Science Foundation of China (Grant No.52174346) and the Natural Science Foundation of Jiangsu Province of China (Grant No. BK20191432).

## References

- B. Lai, Y.F. Li, H.J. Wang, A.H. Li, M.G. Zhu, and W. Li, Quasi-Periodic Layer Structure of Die-Upset NdFeB Magnets, *J. Rare Earth.*, 2013, **31**, p 679–684.
- R.J. Chen, Z.X. Wang, X. Tang, W.Z. Yin, C.X. Jin, J.Y. Ju, D. Lee, and A.R. Yan, Rare Earth Permanent Magnets Prepared by Hot Deformation Process, *Chin. Phys. B*, 2018, **27**, p 117504.

- M. Lin, H.J. Wang, P.P. Yi, and A.R. Yan, Effects of Excessive Grain Growth on the Magnetic and Mechanical Properties of Hot-Deformed NdFeB magnets, *J. Magn. Magn Mater.*, 2010, **322**, p 2268–2271.
- O.M. Ragg, I.R. Harris, H. Nagel, and P. Bohm, Hot Pressing Nd-Fe-B HDDR Powders, *IEEE T. Magn.*, 1996, **32**, p 4395–4397.
- W. Grünberger, D. Hinz, A. Kirchner, K. Müller, and L. Schultz, Hot Deformation of Nanocrystalline Nd-Fe-B Alloys, *J. Alloy. Compd.*, 1997, **257**, p 2748–2752.
- Y.L. Huang, Y.H. Hou, S.C. Ma, Z.C. Zhong, Z.W. Liu, D.C. Zeng, X. Gao, and J. Zhu, Influences of Strain Rate on the Microstructure and Properties for Hot Deformed NdFeB Magnets, *Rare Metal Mat. Eng.*, 2014, **43**, p 1451–1458.
- L. Li and C.D. Graham, Mechanism of Texture Formation by Hot Deformation in Rapidly Quenched FeNdB, *J. Appl. Phys.*, 1990, **67**, p 4756–4758.
- F. Yang, L. You, Z.M. Guo, V. Paley, and A.A. Volinsky, Coercivity Enhancement and Grain Refinement in Nd-Fe-B Sintered Magnets with Pyrite Doping by Jet Milling, *J. Magn. Magn Mater.*, 2019, **469**, p 146–150.
- J. Li, Y. Bian, K. Xu, X.Y. Xie, J.J. Ni, C. Hu, and S.T. Zhou, Improvement of Comprehensive Magnetic Properties for Hot-Deformed NdFeB Magnets Via Intergranular Additions of Nano-TiC, *Mater. Lett.*, 2020, **267**, p 127537.
- Y.H. Hou, Y.L. Wang, Y.L. Huang, Y. Wang, S. Li, S.C. Ma, Z.W. Liu, D.C. Zeng, L.Z. Zhao, and Z.C. Zhong, Effects of Nd-Rich Phase on the Improved Properties and Recoil Loops for Hot Deformed Nd-Fe-B Magnets, *Acta Mater.*, 2016, **115**, p 385–391.
- J.J. Ni, M. Yan, T.Y. Ma, and W. Zhang, Magnetic and Anticorrosion Properties of Two-Powder (Pr, Nd)<sub>12.6</sub>Fe<sub>81.3</sub>B<sub>6.1</sub>-Type Sintered Magnets with Additions of (Pr, Nd)<sub>32.5</sub>Fe<sub>62.0</sub>Cu<sub>5.5</sub>, *Mater. Chem. Phys.*, 2015, **151**, p 126–132.
- H.Y. Li, Z. Hao, Y.H. Liu, W. Zhu, Y.Z. Chen, and J.Y. Duan, Corrosion Behavior of Sintered Nd-Fe-B Magnets, *Rare Metal Mat. Eng.*, 2018, **47**, p 1451–1458.
- S.P. Harrington, F. Wang, and T.M. Devine, The Structure and Electronic Properties of Passive and Prepassive Films of Iron in Borate Buffer, *Electrochim. Acta*, 2010, **55**, p 4092–4102.

**Publisher's Note** Springer Nature remains neutral with regard to jurisdictional claims in published maps and institutional affiliations.

Springer Nature or its licensor (e.g. a society or other partner) holds exclusive rights to this article under a publishing agreement with the author(s) or other rightsholder(s); author self-archiving of the accepted manuscript version of this article is solely governed by the terms of such publishing agreement and applicable law.